International Journal of Geo-Information

MDPI

Article

Change Detection in Coral Reef Environment Using High-Resolution Images: Comparison of Object-Based and Pixel-Based Paradigms

Zhenjin Zhou [1,2], Lei Ma [1,2,*], Tengyu Fu [1,2], Ge Zhang [1,2,3], Mengru Yao [1,2] and Manchun Li [1,2]

1 School of Geography and Ocean Science, Nanjing University, Nanjing 210023, China; mg1627117@smail.nju.edu.cn (Z.Z.); anythinganytime@foxmail.com (T.F.); mg1527116@smail.nju.edu.cn (G.Z.); mengru.yao@foxmail.com (M.Y.); limanchunnju@163.com (M.L.)
2 Jiangsu Provincial Key Laboratory of Geographic Information Science and Technology, Nanjing University, Nanjing 210023, China
3 Shenzhen Urban Planning & Land Resource Research Center, Shenzhen 518028, China
* Correspondence: maleinju@gmail.com; Tel.: +86-182-5195-2382

Received: 28 July 2018; Accepted: 29 October 2018; Published: 12 November 2018

Abstract: Despite increases in the spatial resolution of satellite imagery prompting interest in object-based image analysis, few studies have used object-based methods for monitoring changes in coral reefs. This study proposes a high accuracy object-based change detection (OBCD) method intended for coral reef environment, which uses QuickBird and WorldView-2 images. The proposed methodological framework includes image fusion, multi-temporal image segmentation, image differencing, random forests models, and object-area-based accuracy assessment. For validation, we applied the method to images of four coral reef study sites in the South China Sea. We compared the proposed OBCD method with a conventional pixel-based change detection (PBCD) method by implementing both methods under the same conditions. The average overall accuracy of OBCD exceeded 90%, which was approximately 20% higher than PBCD. The OBCD method was free from salt-and-pepper effects and was less prone to images misregistration in terms of change detection accuracy and mapping results. The object-area-based accuracy assessment reached a higher overall accuracy and per-class accuracy than the object-number-based and pixel-number-based accuracy assessment.

Keywords: coral reef; change detection; very high resolution; object-based method; random forests

1. Introduction

Coral reefs are among the most productive and diverse ecosystems on earth. They provide a series of ecological goods and services for mankind [1], and they are often described as "tropical rainforests of the sea" [2]. However, despite their value, coral reefs globally are facing a crisis [3]. Large swathes of coral reefs have been degraded by overfishing, coastal development, shipping, and climate change [4]. Therefore, it is necessary to improve dynamic monitoring of coral reefs including reef islands, such that coral reef resources can be managed and protected effectively [5].

Remote sensing technology offers the advantages of synoptic perspective, frequent sampling, and easy accessibility. Given the special geographical locations and distribution of coral reefs, remote sensing technology is used commonly as the preferred tool for dynamic monitoring of their changes [6–8]. Landsat satellite images have been used most frequently in remote sensing based studies of coral reefs because they are cost-effective and of adequate accuracy for coarse descriptions of habitat [9]. What's more, most previous studies have employed pixel-based post-classification

methods for coral reef change detection. However, because of the limitations of medium-resolution sensors such as Landsat and SPOT, it is difficult to distinguish coral reef geomorphological dynamics from sea level rise [10], and to detect changes on the scale of a few meters in coral reef habitats [11]. With continued refinement of the spatial resolution of satellite imagery, conventional per-pixel methods have been found susceptible to a number of challenges in relation to change detection, including image misregistration [6,12] and salt-and-pepper effects [13,14]. Coral reef images, lack of distinct and stable texture features, are difficult to be accurately registered to each other [15], which makes the traditional pixel-based approach less promising in coral reef change detection using high-resolution images.

Recent years have seen an increase in the number of studies using object-based image analysis (OBIA) [13]. OBIA has also been applied in coral reef environment, from geomorphological mapping to benthic community discrimination [16–18]. OBIA represents an effective combination of both the contextual analysis of visual interpretation and the quantitative analysis of the pixel-based method [19]. It has been proven that image registration error greatly affects the per-pixel change detection accuracy while the object-based method is less sensitive to image misregistration [20,21]. However, to the best of our knowledge, few studies have used object-based change detection (OBCD) methods in coral reef change detection. Generally, there are two possible strategies for OBCD methods: post-classification comparison and multi-temporal image object analysis [22]. The essence of the post-classification comparison approach lies in the initial classification, i.e., images acquired at different times are classified individually and then overlaid in order to reveal changes that have occurred from one period to another. Although this approach can provide "from-to" change information, the change detection accuracy depends on the performance of the initial image classification and differences in the segmentation of time series images could induce sliver changes [23]. In multi-temporal image object analysis, multi-date images are segmented simultaneously to ensure the segmentations are spatially consistent, and changes are usually identified via statistical or threshold methods [24,25]. However, the outputs of such methods are simply "changed or unchanged" binary images that lack precise information on the types of change [26]. Given all these facts above, in this study, direct multi-date image classification using a machine learning algorithm was conducted on coral reef image objects to process large quantities of attribute features autonomously and provide information on the specific changes as well.

Since the original proposal of OBIA, numerous studies have compared pixel-based and object-based paradigms, mainly in cropland mapping, rural-urban land cover classification, plant mapping, etc. [27–29]. But, only a few of them concentrated on coral reef environment. Benfield et al. [30] compared an object-oriented nearest neighbor classifier and a pixel-based maximum likelihood classifier in coral reef mapping for the very first time, and found that the OBIA method yielded higher accuracy in mapping coral reef habitats. Phinn, Roelfsema, and Mumby [17] assigned categories to coral reef image objects by setting membership rules iteratively and then compared the object-based analysis with a supervised pixel-based classification. However, these studies focused on coral reef mapping and classification rather than coral reef change detection. Besides, they adopted diverse approaches to compare pixel-based and object-based paradigms, which are sometimes site-specific or rely on the datasets (i.e., data distribution) [31].

The primary objectives of this study are: (1) to propose a multi-temporal OBCD method combined with random forests (RF) and directly recognize changes and change types in coral reef study sites using high-resolution satellite images; (2) to compare the effectiveness of OBCD and pixel-based change detection (PBCD) method in coral reef change detection, using both point-based accuracy assessment and geometric accuracy assessment. We selected four coral reef study sites in the Spratly Islands of the South China Sea, and we acquired QuickBird and WorldView-2 satellite images as experimental data. The remainder of this paper is organized as follows: Section 2 gives detailed information on both study sites and data set, and elaborates on the methodology of this study; Section 3, Section 4, and Section 5 respectively present the results, discussion, and conclusions.

2. Materials and Methods

2.1. Study Area

The South China Sea, which encompasses an area of more than 3 million km^2, is the western margin of the Pacific Ocean and the third largest marginal sea in the world. The coastal areas of the South China Sea and its archipelagoes (e.g., the Spratly Islands) provide highly favorable conditions for the growth and development of coral reefs. This region supports 571 known species of reef coral, a richness in biodiversity comparable with that of the Coral Triangle [32]. However, in recent years, the reef islands within this region have undergone complex changes due to both the construction of artificial islands and the effects of natural factors. Therefore, monitoring and studying of the changes in the coral reef environment are very important for marine conservation and management. In this study, we chose Taiping Island, Zhongye Island, and two segments of Barque Canada Reef as study sites (Figure 1), and we monitored dynamics of the reef islands and of the benthic coral habitats.

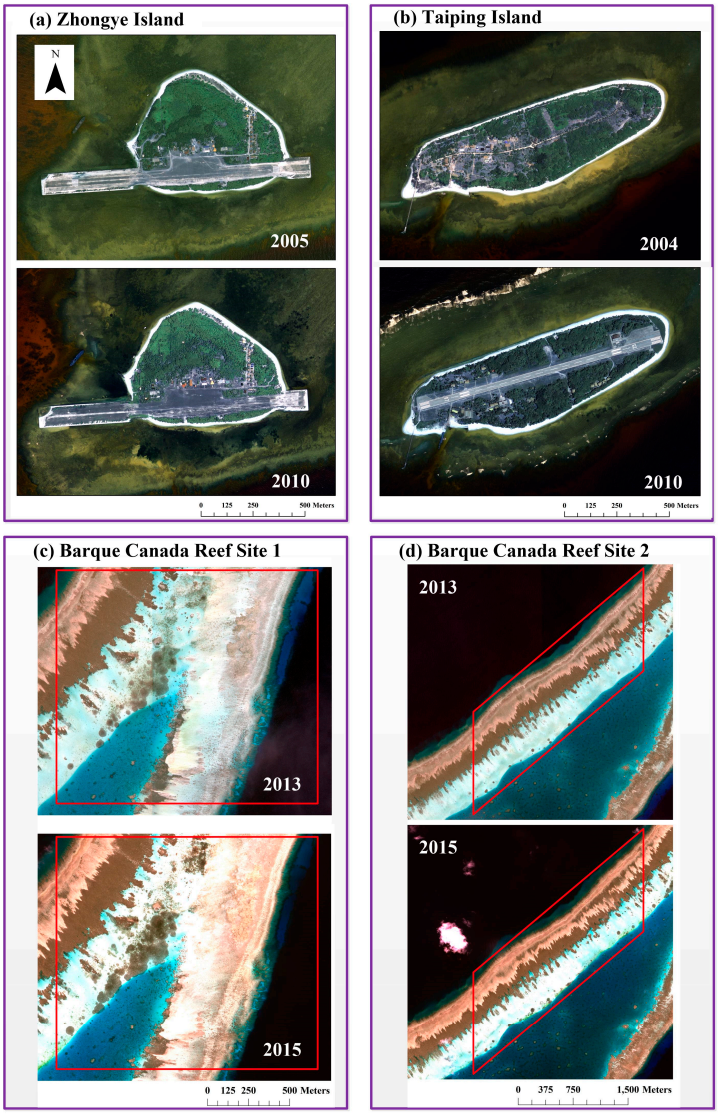

Figure 1. Four coral reef study sites: (**a**,**b**) QuickBird satellite images of Taiping Island and Zhongye Island (Bands 3, 2, and 1 in RGB); (**c**,**d**) WorldView-2 satellite images of Barque Canada Reef (Bands 5, 3, and 2 in RGB), where red rectangles indicate the two study sites in Barque Canada reef.

Zhongye Island (11°03′6″ N, 114°17′12″ E) is of triangular shape, covering an area of roughly 0.372 km^2. Zhongye Island has a long history of habitation by fishermen. The island is covered by tropical coastal forests, grasslands, beaches formed by the accretion of carbonate sands and coral shingles, buildings, and roads.

Taiping Island (10°22′37″ N, 114°21′57″ E), located in the northern central region of the Spratly Islands, is a long and narrow island with East-West alignment. The length of the island is approximately 1.4 km and its width is about 0.4 km. Its terrain is low and flat with elevations ranging from 4.0 to 6.0 masl. The land cover types on Taiping Island are similar with Zhongye Island.

Barque Canada Reef (8°10′50″ N, 113°17′41″ E) is an ovular reef that is 33-km long and 5-km wide at its maximum. Its overall area is approximately 66.4 km^2 (of which reef flat accounts for 49.5 km^2), making it one of the largest of the Spratly Islands. The broad and shallow reef lagoon in the middle of Barque Canada Reef (depth: 1.5–3.0 m) is one of the most important fisheries in the Spratly Islands. Two parts of Barque Canada Reef were selected as study sites for this work. Detailed information (i.e., area of different surface types) of all study sites has been illustrated in Table A1 in Appendix A.

2.2. Data Set and Image Preprocessing

The focus of this study is bi-temporal change detection, so images with pronounced changes between two different times were needed. However, due to the special marine environment and the monsoonal climate [33], the satellite images of the study sites suffered a lot from cloud and aerosol. We have tried to select cloud-free and high-quality images with the data acquisition month close to each other (an interval less than 2 months) in case of pseudo changes or detection errors. Finally, six satellite images over the four study sites were selected as the best available cloud-free scenes, including QuickBird images of Taiping Island acquired in April 2004 and February 2010, QuickBird images of Zhongye Island acquired in April 2005 and June 2010, and WorldView-2 images of Barque Canada Reef acquired in May 2013 and July 2015 (Table 1).

Table 1. Satellite images' information specific to the study sites.

Parameter	Zhongye Island	Taiping Island	Barque Canada Reef
Data	22 April 2005 8 June 2010	14 April 2004 20 February 2010	20 May 2013 24 July 2015
Sensor	QuickBird	QuickBird	WorldView-2
Spatial resolution (m)	MS [1]: 2.4 PAN [2]: 0.6	MS: 2.4 PAN: 0.6	MS: 2.0 PAN: 0.5
Spectral band (μm)	Blue: 0.45–0.52 Green: 0.52–0.60 Red: 0.63–0.69 Near IR: 0.76–0.90	Blue: 0.45–0.52 Green: 0.52–0.60 Red: 0.63–0.69 Near IR: 0.76–0.90	Coastal: 0.400–0.450 Blue: 0.450–0.510 Green: 0.510–0.580 Yellow: 0.585–0.625 Red: 0.630–0.690 Red Edge: 0.705–0.745 NIR1: 0.770–0.895 NIR2: 0.860–1.040

[1] MS: multispectral. [2] PAN: panchromatic.

Radiometric correction was firstly conducted for all the images, which is a critical pre-process for change detection. In this study, the digital number values of the satellite images were firstly converted to physically meaningful top-of-atmosphere radiances via radiometric calibration toolbox, following which they were transformed into surface reflectance, using a MODTRAN-based atmospheric algorithm, Fast Line-of-Sight Atmospheric Analysis of Spectral Hyper-cubes (FLAAH) module developed by Spectral Science, Inc., Burlington, NJ, USA. [34]. A further description of atmospheric correction process is provided by the user's guide [35]. The Gram–Schmidt algorithm was used to fuse the low-resolution multispectral bands with the high-resolution panchromatic band, which resulted

in synthetic data with high spatial detail and spectral diversity [36]. For each study site, the image from the earlier time point was registered to the one from the later time point using the ENVI Image Registration Workflow tool, which achieved a registration error of <2 pixels. In this process, tie points were generated automatically according to the geographical coordinates of the images, and a first-order polynomial transformation and nearest neighbor resampling were applied to the earlier image. The accuracy of monitoring and mapping of shallow-water coral reefs is usually compromised by variable water depths. To overcome the influence of bottom reflectance, a kind of depth-invariant index was proposed for water column correction [37]. However, as the study sites of Barque Canada Reef are reasonably shallow (depth: 1.5–3.0 m), water column correction was deemed unnecessary in such case [38]. Furthermore, as the focus of this study was on the detection of relative changes between two periods, the effects of water depth were deemed negligible.

All the six remote sensing images were interpreted visually by digitalizing and classifying the whole scenes. Then, we overlaid two digitalized images of each study site and generated a new layer. In the generated layer, polygons with attributes from two different times were defined as "no change" or as a certain change category according to its types in two different times. The definition rules of two reef islands are shown in Table 2 and those of Barque Canada Reef are shown in Table 3. In the reef islands, change categories include vegetation deterioration, vegetation growth or plantation, coastal accretion, sea level rise or coastal erosion, and others. The "others" category refers to changes related to buildings and infrastructure construction, e.g., house building, runway or road construction, coastal harbor construction, etc. Areas without surface type change were categorized as "no change". In the Barque Canada Reef study sites, changes refer to alterations in species assemblages and in their associated substrata extent [39]. These changes were categorized as aquatic vegetation growth, algae growth, reef sediments extension, and algae degradation. Areas without habitat type change were categorized as "no change". After defining the change categories, the overlaid layer of each study site was used as reference data for sampling in both OBCD and PBCD methods and for object-area-based accuracy assessment. The area and proportion of each change category in all study sites are displayed in Tables A2 and A3 in Appendix A.

Table 2. Change category definition of Zhongye Island and Taiping Island.

Surface Type in Time 1	Surface Type in Time 2	Change Category
Vegetation	Buildings and infrastructures	Vegetation deterioration
	Bare land	
	Beach	
	Ocean	Sea level rise or coastal erosion
Beach	Buildings and infrastructures	Others
	Ocean	Sea level rise or coastal erosion
	Vegetation	vegetation growth or plantation
Ocean	Buildings and infrastructures	Others
	Beach	Coastal accretion
	Vegetation	Vegetation growth or plantation
Buildings and infrastructures	Vegetation	Vegetation growth or plantation
	Bare land	Others
Bare land	Beach	Coastal accretion
	Ocean	Sea level rise or coastal erosion
	Vegetation	Vegetation growth or plantation
	Buildings and infrastructures	Others

Table 3. Change category definition of Barque Canada Reef.

Habitat Type in Time 1	Habitat Type in Time 2	Change Category
Sand	Algae-dominated	Algae growth
Sand	Aquatic vegetation	Aquatic vegetation growth
Rubble-dominated	Coral-dominated	Reef sediments extension
Algae-dominated	Sand	Algae degradation

A detailed schematic of all experimental procedures including image preprocessing has been presented in Figure 2. Compared to PBCD, the OBCD method includes an additional key step of image segmentation, which is described in detail in Section 2.3.1. Finally, the change detection performances of the two methods are compared in terms of the overall accuracy (OA), Producer's accuracy (PA), User's accuracy (UA), Kappa coefficient (KA), and Z-test.

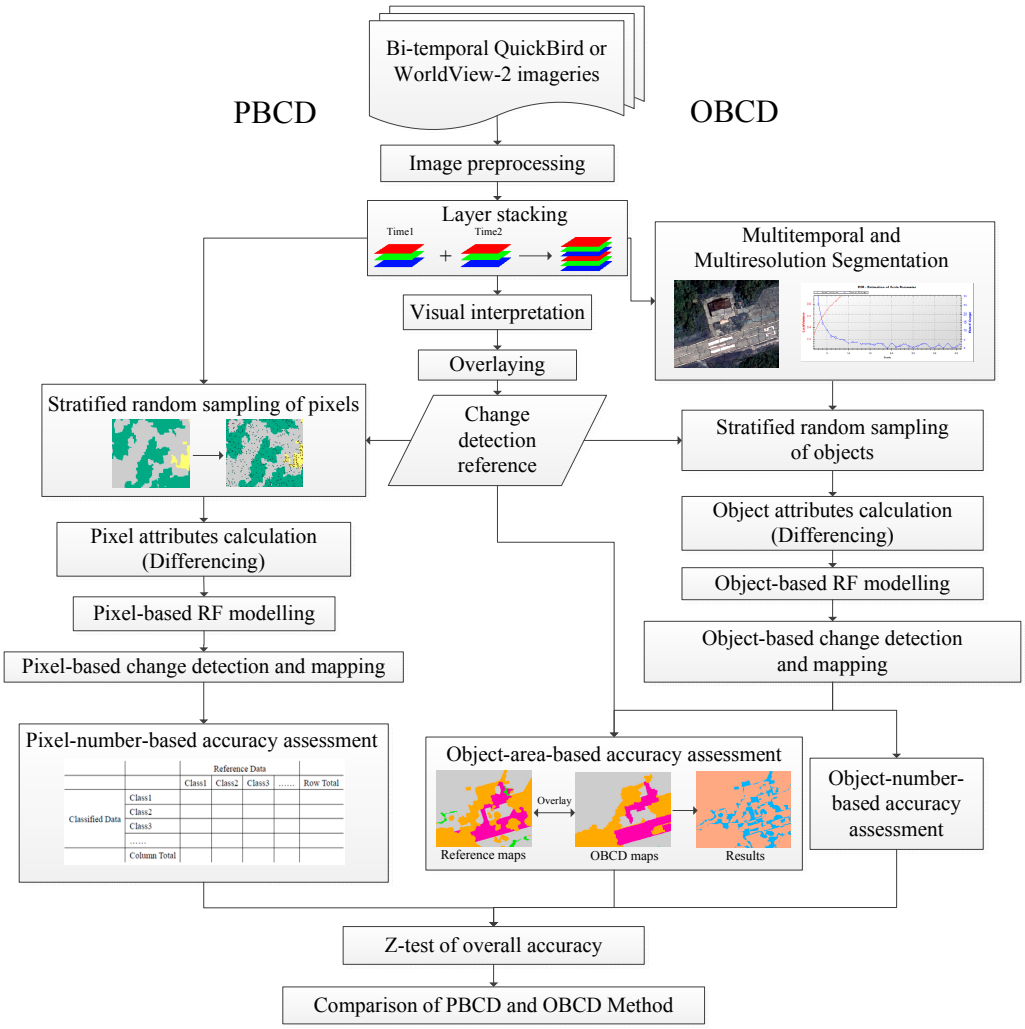

Figure 2. Schematic of the procedures implemented in coral reef change detection using the pixel-based change detection (PBCD) and object-based change detection (OBCD) methods and the comparison of their results.

2.3. Object-Based Coral Reef Change Detection

2.3.1. Multi-Temporal Segmentation

Image segmentation is at the core of the OBIA method because the object obtained from image segmentation is the basic unit used for image classification or change detection. Thus, the quality of image segmentation is correlated strongly with the accuracy of image classification and change detection [40]. Multiresolution segmentation is a regional merging algorithm that forms an image object starting from a single pixel. At each step, a pair of small image objects will be selected for merging into a larger object or not based on a homogeneity criterion that is defined by the scale parameter (SP), color/shape weight, and smoothness/compactness weight. As the SP determines the average size of the image objects according to the heterogeneity within the object, the SP selection is crucially important [41]. Based on the rate of change of local variance (ROC-LV) concept [42], an automatic tool called "Estimate of Scale Parameter" (ESP) has been proposed as particularly suitable for replacing the subjective trial-and-error method in SP selection [43,44]. The local variance (LV) value reflects the heterogeneity within an object. Its value increases incrementally with the increasing segmentation scale up to a point, at which the ROV-LV reached a peak. The SP at this point is considered the optimal segmentation scale and the object obtained from the segmentation approximates the actual ground object.

In this work, segmentation was conducted on all images of different dates simultaneously after stacking all sets of the spectral bands. This multi-temporal image segmentation approach unifies the object boundaries of all sequential images, minimizing sliver errors and delineating objects that are composed of spatially adjacent pixels with similar spectral properties over time [19,45].

The ESP tool has been programmed in CNL within the eCognition® Developer 9.0 environment. The ESP2 plugin in eCognition® Developer 9.0 was used to perform multiresolution segmentation in a hierarchical manner with default scale increments of 1, 10, and 100 and a step size of 1. The values of shape weight and compactness weight were set as 0.1 and 0.5, respectively. ROC-LV curves were produced using standalone software. As an example, the optimal segmentation scale of Zhongye Island was established as 13, as was shown in Figure 3.

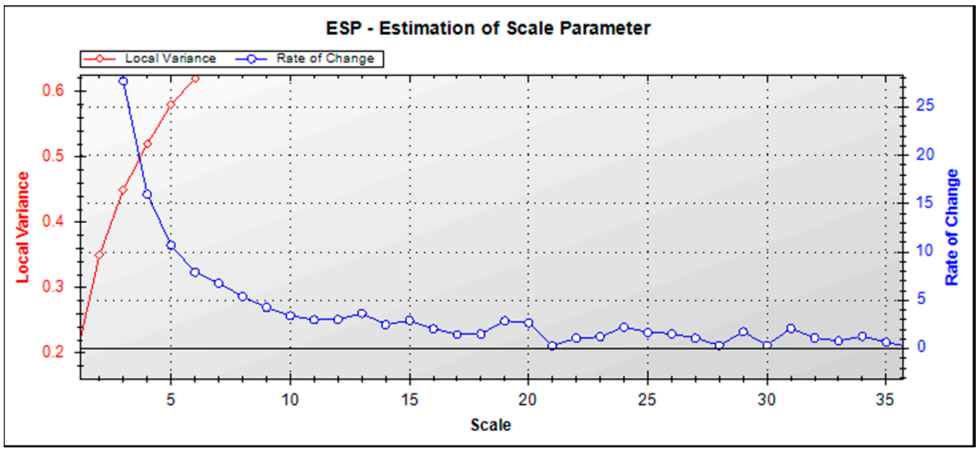

Figure 3. Rate of change of local variance (ROC-LV) curve of multiresolution segmentation of Zhongye Island images.

2.3.2. Object Feature Selection and Calculation

Each image object has its own spectral, spatial, and textural features that are fundamental elements in human interpretation of color photographs [46]. The state of each object at different time points can be described using a given set of features [47]. In Equation (1), S_{t1} represents the state (or land cover type) of an object at time t_1, and $F_1, F_2, \ldots F_n$ is the feature set of t_1. S_{t2} represents the state (or

land cover type) of an object at time t_2, and F_1', F_2', ... F_n' is the feature set of t_2. ΔS is the difference between the features of the object at t_1 and t_2. Using feature differences to train the change detection model halves the dimensionality of the dataset and reduces the necessary computations [48].

$$S_{t_1} = \begin{pmatrix} F_1 \\ F_2 \\ F_3 \\ \vdots \\ F_n \end{pmatrix} S_{t_2} = \begin{pmatrix} F_1' \\ F_2' \\ F_3' \\ \vdots \\ F_n' \end{pmatrix} \Delta S = \begin{pmatrix} F_1 - F_1' \\ F_2 - F_2' \\ F_3 - F_3' \\ \vdots \\ F_n - F_n' \end{pmatrix} \quad (1)$$

After multi-temporal segmentation, the objects in the segmented images have consistent geometries and sizes between different times. Hence, only the spectral and textural features of each object were considered for change detection. For better recognition of changes in vegetation and water bodies, the Normalized Difference Vegetation Index (NDVI) [49] and Normalized Difference Water Index (NDWI) [50] were calculated as additional feature bands for both Taiping Island and Zhongye Island using band algebra. The object features of both Zhongye Island and Taiping Island included the mean values and standard deviations of the blue, green, red, near infrared, NDVI, and NDWI bands. Haralick texture features including GLCM homogeneity, GLCM contrast, GLCM dissimilarity, GLCM entropy, GLCM Ang. 2nd moment, GLCM correlation, GLDV Ang. 2nd moment, GLDV entropy, and GLDV contrast [51]. As the study sites on Barque Canada Reef were located in shallow water, we calculated only the mean values and standard deviations of the three visible bands, i.e., the blue, green, and red bands that can penetrate shallow water [30], together with the nine Haralick texture features. All these features were calculated in eCognition® Developer 9.0.

2.3.3. Sampling Changed Objects

In order to implement stratified random sampling, we first labelled all segmented objects using a maximum overlay rule with reference layer, where all changes or no changes are depicted for individual study site (see Section 2.2). Each segmented object was defined as the class displayed in the reference layer that covered the majority area of this object. Subsequently, all segmented objects were divided into groups according to their change types. Then, each stratum was randomly sampled with the same training set ratio of 30%. For Zhongye Island, 902 segmented objects were selected for training samples. For Taiping Island, 1101 segmented objects were selected for training samples. The training samples of the two study sites in Barque Canada Reef were 2843 and 3436 image objects, respectively. The remaining 70% objects were used as validation samples. Sample numbers of each change category have been displayed in Tables A4 and A5. As the sampled units were polygonal objects, there could have been variety in the training sample objects' size. Therefore, we made appropriate adjustments to the sampling results through visual observation, such that the training samples were representative both in change type and in size.

2.3.4. Recognizing Changed Objects Using the RF Algorithm

The RF algorithm [52] is a powerful ensemble learning technique that has been used widely in remote sensing image classification [53,54]. Its superiority to other machine learning methods (e.g., decision tree classifier, neural network classifier, maximum likelihood classifier, etc.) has been demonstrated in a number of earlier studies [53,55,56]. In a lot of studies, RF classifier performed equally well to SVMs in terms of classification accuracy and training time [57–59], but RF was acknowledged more user-friendly for the number of user-defined parameters required by RF classifiers is less than the number required for SVMs and easier to define [60]. The RF algorithm has not only been applied successfully in pixel-based image analyses, but has also shown great promise in the OBIA method for its high accuracy [61] and robustness to training sample reduction and feature selection [62,63]. Therefore, the RF algorithm was adopted in the current work.

The RF algorithm was implemented in the RandomForest package in the R environment [64]. The input predictive variables were difference values of object features between two time points, including the difference of mean values and standard deviations of the blue, green, red, near infrared, NDVI, and NDWI bands, the Haralick texture features, as was mentioned above. The predicting result was the change category. Before training a RF model, two primary parameters of RF algorithm need to be defined: the number of trees *ntree* and the number of split variable parameters *mtry*. A review of RF application in remote sensing concluded that in most studies, the errors stabilize before *ntree* value reaches 500, so the default value of 500 for *ntree* is an acceptable value [65]. The other parameter *mtry* is the number of prediction variables used in each node to make the tree grow. According to Rodriguez-Galiano, et al. [66], a RF is not sensitive to the value of *mtry* as the generalization error converges from the value of approximately 100 trees. Moreover, it was found that using a univariate RF algorithm could produce good accuracy and save computation time [52]. Therefore, this paper set *ntree* as 500 and set *mtry* as 1. In this study, four separate RF models were established to detect changes in four study sites.

2.4. Pixel-Based Coral Reef Change Detection

The same fundamental procedures (e.g., stratified random sampling and RF change detection) were used in the PBCD method, with the exception of image segmentation. Here the basic unit of the PBCD method is a pixel rather than an object. Therefore, we directly sampled the pixels labelled by the reference layer for each category, and each stratum was randomly sampled with the same training set ratio as object-based method. Subsequently, the training samples and validation samples of each change category were collected based on the same proportion as object-based method (still 30% training samples and 70% validation samples for each category). In this process, a total number of 42,276 pixels and 69,846 pixels were selected in Taiping Island and Zhongye Island, respectively. A total number of 460,960 pixels and 459,120 pixels were selected in Barque Canada Reef Site 1 and Site 2. The sample numbers of each change category in all the study sites have been shown in Tables A6 and A7. The pixel-based RF change detection models were also trained and constructed using the RandomForest package in the R environment with the parameter *ntree* set as 500 and the parameter *mtry* set as 1. For Zhongye Island and Taiping Island, the pixel value difference of the blue, green, red, near infrared, NDVI, and NDWI bands was input as predictive variables to predict change types. For the study sites on Barque Canada Reef, the pixel value difference of the blue, green, and red bands was chosen as predictive variables. Ultimately, we obtained change detection results for the entire image of each study site with the aid of RF change detection models.

2.5. Accuracy Assessment and Statistical Comparisons

2.5.1. Confusion Matrix Based on Pixel Number, Object Number, and Object Area

For each of the four study sites, three confusion matrices were created based on pixel number, object number, and object area in order to calculate the OA, PA, UA, and Kappa coefficient. In the PBCD method, the values in the rows and columns of the confusion matrices refer to pixel numbers. To analyze quantitatively the classification quality of object-based methods, Laliberte and Rango [67] considered each object as an element, and generated confusion matrices based on the object numbers. However, this method was deemed spatially implicit [68]. Thematic accuracy and completeness as well as geometric quality and integrity were suggested prerequisites for comprehensive analysis of object-based classification quality [69]. Whiteside, et al. [70] proposed an area-based validation method, in which reference layer R is superimposed on the change detection product C. Their overlap, $|C_i \cap R_i|$ represents the correctly identified part of change type *i*, whereas $|C_i \cap \neg R_i|$ represents the commission part of change type *i* and $|\neg C_i \cap R_i|$ is the omission part of change type *i*. In this case, the values in the rows and columns of the confusion matrices refer to the areas of these parts. In this work,

a pixel-number-based confusion matrix was used to assess the PBCD accuracy, whereas confusion matrices based on object number and object area were used to assess the OBCD accuracy.

2.5.2. Statistical Hypothesis Test for PBCD and OBCD Accuracy Assessment

To determine whether the RF change detection models in the PBCD and OBCD methods yielded significantly better results than random ones, a Z-test was performed on the Kappa coefficient of each confusion matrix. In addition, the Kappa coefficients of the OBCD and PBCD confusion matrices were analyzed using a Z-test. This was performed to check for significant differences between the accuracies of the two methods [71] in order to determine whether the OBCD method was significantly superior.

Here, K_1 and K_2 denote the KA coefficients of the two confusion matrices, while var (K_1) and var (K_2) denote the variances of K_1 and K_2, respectively. The Z-test statistic for testing the significance of a single confusion matrix is calculated as follows:

$$Z_1 = \frac{K_1}{\sqrt{\text{var}(K_1)}} \tag{2}$$

where Z_1 is a standard normal deviate. The null and alternative hypotheses are formulated as follows: H_0: $K_1 = 0$, H_1: $K_1 \neq 0$; H_0 is rejected if $Z \geq Z_{\alpha/2}$, where a/2 is the confidence level.

The Z-test statistic for testing whether two independent confusion matrices are significantly different can be expressed as

$$Z_{12} = \frac{|K_1 - K_2|}{\sqrt{\text{var}(K_1) + \text{var}(K_2)}} \tag{3}$$

where Z_{12} is a standard normal deviate. The null and alternative hypotheses are formulated as follows: H_0: $(K_1 - K_2) = 0$, H_1: $(K_1 - K_2) \neq 0$; H_0 is rejected if $Z \geq Z_{\alpha/2}$.

At the 95% (99%) confidence level, the critical value would be 1.96 (2.58). For a single confusion matrix test, a value of the Z statistic > 1.96 means the result is significant (i.e., better than random) at the 95% confidence level. For a test between two confusion matrices, a value of the Z statistic > 1.96 means the results are significantly different, i.e., one method outperformed the other.

3. Results

3.1. Visual Examination of PBCD and OBCD Maps

The outputs of the change detection methods for the four study sites are shown in Figures 4 and 5. Visual comparison revealed that both the OBCD and the PBCD methods were able to recognize changed areas and change types. Nonetheless, the OBCD method appeared to outperform the PBCD method. Specifically, the OBCD maps were not affected severely by salt-and-pepper effects and very few unchanged areas were misidentified as changed.

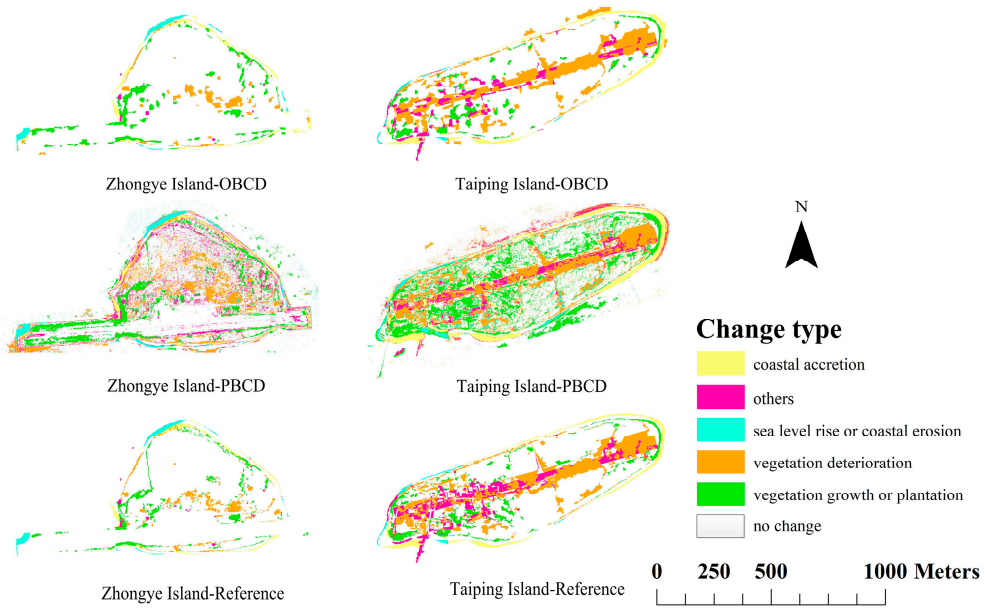

Figure 4. Change detection maps and reference maps of Zhongye Island and Taiping Island.

3.1.1. An Observation of PBCD Maps

The changed areas recognized by the PBCD method were irregular clusters of pixels. Furthermore, pixels of various change types were distributed sporadically within the areas of certain other change types. For example, the areas of "vegetation deterioration" detected on both Taiping Island and Zhongye Island also contained scattered pixels of the "others" change type. We also found that PBCD frequently detected unchanged areas as changed. On both Taiping Island and Zhongye Island, the surrounding stable (unchanged) marine areas were identified as "vegetation growth or plantation", "vegetation deterioration", and "others". A proportion of unchanged forest on Zhongye Island was identified as "vegetation deterioration" and "others", while central areas of Taiping Island, where no change occurred, were detected mostly as "vegetation growth or plantation". The PBCD method presented the worst visual accuracy for both study sites of Barque Canada Reef. In Barque Canada Reef Site 1, large areas of "no change" type were misidentified as "aquatic vegetation growth" and "algae growth", while substantial proportions of "no change" areas in Barque Canada Reef Site 2 were misidentified as "aquatic vegetation growth".

3.1.2. An Observation of OBCD Maps

In stark contrast to the PBCD method, the OBCD method produced much cleaner and neater change detection maps with the polygon as its basic analysis unit. Of the four study sites, the change detection map of Zhongye Island was found most similar with its reference layer, although minor changes such as vegetation growth on narrow paths were not detected well. The change detection map for Taiping Island was also satisfactory, except that some unchanged marine areas to the north of the reef island were misidentified as "vegetation deterioration" shown as conspicuous orange patches. Patches of unchanged area in eastern parts of Barque Canada Reef Site 1were misidentified as "algae growth", while a scattering of unchanged polygons in the middle of Barque Canada Reef Site 2 were detected as "aquatic vegetation growth". The results revealed that the primary weakness of the OBCD method was that there were discrepancies between the boundaries of its change detection units (image objects) and the polygonal boundaries in the reference layer, which delimited the actual change extent.

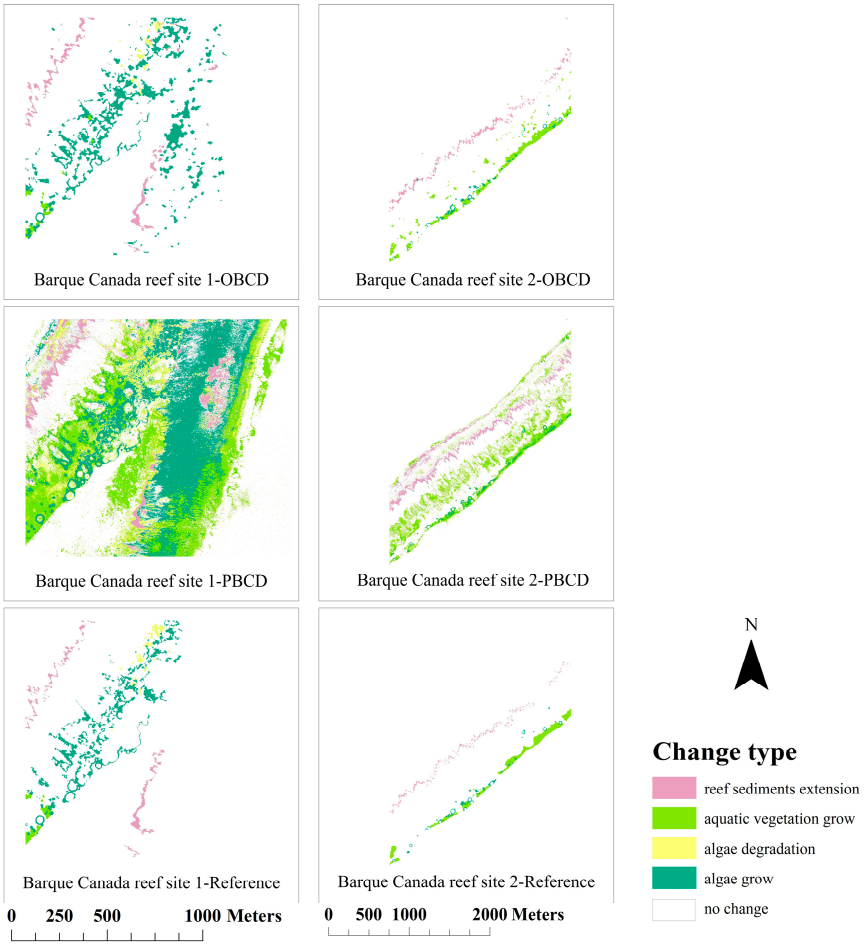

Figure 5. Change detection maps and reference maps of the two study sites on Barque Canada Reef.

3.2. Quantitative Evaluations of PBCD and OBCD Performances

3.2.1. PBCD and OBCD Accuracy Assessment

Three confusion matrices based on pixel number, object number, and object area were used to assess the accuracy of each change detection result. Figure 6 illustrates the OAs and the Kappa coefficients of the OBCD and PBCD methods for each study site. Tables 4–7 display all the confusion matrices. It was found that the OAs of OBCD, either object-number or object-area based, were greatly higher than those of PBCD for all the study sites. Meanwhile, the object-area-based OA was a little bit higher than the object-number-based OA. The average OA of OBCD over the four study sites was >90%, i.e., approximately 20% higher than the average OA of PBCD (69.72%). The OBCD method was effective for the reef islands and coral reef habitats change detection, achieving OAs > 90%, except for Taiping Island, whose OA was only slightly >85%. The accuracy assessment results revealed that the PBCD method did worse in benthic coral reef environment than in reef islands. This was particularly reflected in the PBCD Kappa coefficients of the two reef islands and the Barque Canada Reef study sites.

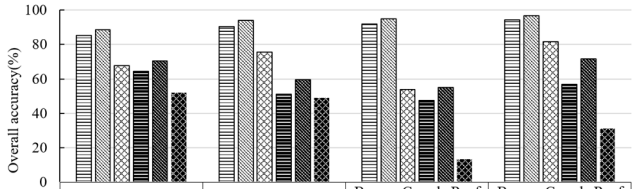

	Taiping Island	Zhongye Island	Barque Canada Reef site 1	Barque Canada Reef site 2
OA(Object number-based)	85.27	90.47	91.92	94.33
OA(Object area-based)	88.56	93.92	94.97	96.71
OA(Pixel number-based)	67.62	75.69	53.94	81.64
KA(Object number-based)	64.47	51.22	47.50	56.98
KA(Object area-based)	70.35	59.50	55.08	71.66
KA(Pixel number-based)	51.95	48.99	13.26	31.26

Figure 6. Overall accuracy and Kappa coefficients of the PBCD and OBCD results of the four study sites.

The PBCD results of all the study sites indicated that the UAs for all change types (except "no change") were <60%, i.e., the commission errors of PBCD were >40%. In Barque Canada Reef study sites, except for "no change" category, the other change categories got greatly worse pre-class UAs. For example, the UA of "reef sediments extension" type was only 24.9% in Barque Canada Reef Site 1 while the "no change" type got a high UA (99.3%). Although per-class UAs of certain categories in object-number-based accuracy assessment were higher than those of pixel-number-based accuracy assessment, some of the rest categories got even lower UAs. In the object-area-based accuracy assessment, the UAs of all the other change types were lower than "no change" type. Nonetheless, per-class UAs of all change categories were higher than those obtained from the object-number-based and pixel-number-based confusion matrices. What's more, the area-based assessment produced a much more balanced per-class UAs of all change categories. For example, in Taiping Island, area-based UAs of all change categories approximated 70%. For the Barque Canada Reef study sites, UAs of all change categories were greatly improved and much closer to each other.

In the change detection results of the two reef island sites, the "others" category consistently displayed the lowest accuracy. Many changes in the "others" category were identified erroneously as "no change", "vegetation deterioration", or "vegetation growth or plantation". For Zhongye Island, the UA of the "others" type was relatively low, i.e., the PBCD method had a UA of 2.9%. In the validation samples of object-number-based accuracy assessment, not a single "other" category object was correctly recognized. The confusion matrices of the OBCD method revealed that "aquatic vegetation growth" and "algae growth" were difficult to distinguish from one another, because the UAs of the OBCD method for "aquatic vegetation growth" and "algae degradation" were relatively low, and the object-number-based accuracy was even lower than the object-area-based accuracy.

Table 4. Confusion matrices of PBCD and OBCD results for Zhongye Island.

Zhongye Island	Reference						
Pixel Number	**Coastal Accretion**	**No Change**	**Others**	**Sea Level Rise or Coastal Erosion**	**Vegetation Deterioration**	**Vegetation Growth or Plantation**	**Total**
Coastal accretion	768	423	27	0	119	14	1351
No change	84	17,882	42	18	311	821	19,158
Others	52	1499	55	3	108	157	1874
Sea level rise or coastal erosion	55	272	5	416	62	0	810
Vegetation deterioration	66	1305	15	3	1113	46	2548
Vegetation growth or plantation	33	1552	25	6	71	2165	3852
Total	1058	22,933	169	446	1784	3203	29,593
PA (%)	72.6	78	32.5	93.3	62.4	67.6	
UA (%)	56.9	93.3	2.9	51.4	43.7	56.2	
Object Number	**Coastal Accretion**	**No change**	**Others**	**Sea level rise or Coastal Erosion**	**Vegetation Deterioration**	**Vegetation Growth or Plantation**	**Total**
Coastal accretion	28	56	0	0	1	0	85
No change	10	2193	4	2	11	15	2235
Others	0	0	0	0	0	0	0
Sea level rise or coastal erosion	0	11	0	24	0	0	35
Vegetation deterioration	1	28	1	0	36	0	66
Vegetation growth or plantation	0	98	0	0	0	50	148
Total	39	2386	5	26	48	65	2569
PA (%)	71.8	91.9	0	92.3	75	76.9	
UA (%)	32.9	98.1	0	68.6	54.6	33.8	
Object Area (m^2)	**Coastal Accretion**	**No Change**	**Others**	**Sea level Rise or Coastal Erosion**	**Vegetation Deterioration**	**Vegetation Growth or Plantation**	**Total**
Coastal accretion	5598.2	5030.4	40.1	1.0	339.0	171.2	11,179.9
No change	1575.5	548,933.2	474.1	465.3	6150.1	7051.3	564,649.3
Others	2.1	162.3	904.0	0.0	57.5	38.4	1164.3
Sea level rise or coastal erosion	107.8	1162.9	2.4	4866.3	21.0	0.0	6160.4
Vegetation deterioration	75.4	5054.5	29.6	0.0	9404.8	71.9	14,636.2
Vegetation growth or plantation	175.9	13,293.7	129.7	0.0	180.1	12,129.0	25,908.3
Total	7534.8	573,636.9	1580.0	5332.5	16,152.5	19,461.8	623,698.4
PA (%)	74.3	95.7	57.2	91.3	58.2	62.3	
UA (%)	50.1	97.2	77.6	79	64.3	46.8	

Table 5. Confusion matrices of PBCD and OBCD results for Taiping Island.

Taiping Island	Reference						
Pixel Number	**Coastal Accretion**	**No Change**	**Others**	**Sea Level Rise or Coastal Erosion**	**Vegetation Deterioration**	**Vegetation Growth or Plantation**	**Total**
Coastal accretion	2552	1159	284	3	410	53	4461
No change	153	21,155	453	26	1092	538	23,417
Others	76	724	1188	5	747	27	2767
Sea level rise or coastal erosion	24	759	200	708	237	131	2059
Vegetation deterioration	49	2423	461	36	4435	80	7484
Vegetation growth or plantation	41	4623	625	56	338	3021	8704
Total	2895	30,843	3211	834	7259	3850	48,892
PA (%)	88.2	68.6	37	84.9	61.1	78.5	
UA (%)	57.2	90.3	42.9	34.4	59.3	34.7	
Object Number	**Coastal Accretion**	**No Change**	**Others**	**Sea Level Rise or Coastal Erosion**	**Vegetation Deterioration**	**Vegetation Growth or Plantation**	**Total**
Coastal accretion	60	37	6	0	0	0	103
No change	5	1479	45	4	48	33	1614
Others	0	5	30	2	7	0	44
Sea level rise or coastal erosion	0	3	0	5	0	0	8
Vegetation deterioration	1	34	39	1	179	1	255
Vegetation growth or plantation	0	38	1	0	0	42	81
Total	66	1596	121	12	234	76	2105
PA (%)	90.9	92.7	24.8	41.7	76.5	55.3	
UA (%)	58.3	91.6	68.2	62.5	70.2	51.9	
Object Area (m^2)	**Coastal Accretion**	**No Change**	**Others**	**Sea Level Rise or Coastal Erosion**	**Vegetation Deterioration**	**Vegetation Growth or Plantation**	**Total**
Coastal accretion	14,814.0	3941.3	480.3	4.3	0.0	14.4	19,254.2
No change	1681.9	531,685.4	8714.4	647.4	16,714.3	11,431.4	570,874.9
Others	100.1	2496.6	17,754.6	187.6	3472.3	476.3	24,487.5
Sea level rise or coastal erosion	1.5	484.7	31.6	1791.2	0.1	0.0	2309.1
Vegetation deterioration	103.0	14,283.9	9323.4	182.7	60,621.0	368.9	84,882.8
Vegetation growth or plantation	60.9	6555.8	597.7	0.0	341.5	13,696.1	21,252.1
Total	16,761.5	559,447.6	36,902.0	2813.2	81,149.3	25,987.1	723,060.5
PA (%)	88.4	95	48.1	63.7	74.7	52.7	
UA (%)	76.9	93.1	72.5	77.6	71.4	64.5	

Table 6. Confusion matrices of PBCD and OBCD results for Barque Canada Reef Site 1.

Barque Canada Reef Site 1	Reference					
Pixel Number	**Reef Sediments Extension**	**Aquatic Vegetation Growth**	**Algae Degradation**	**Algae Growth**	**No Change**	**Total**
Reef sediments extension	3289	0	111	31	9802	13,233
Aquatic vegetation growth	97	988	169	2595	58,638	62,487
Algae degradation	631	35	1100	354	17,922	20,042
Algae growth	26	68	25	11,380	56,983	68,482
No change	190	7	101	849	157,281	158,428
Total	4233	1098	1506	15,209	300,626	322,672
PA (%)	77.7	90	73	74.8	52.3	
UA (%)	24.9	1.6	5.5	16.6	99.3	
Object Number	**Reef Sediments Extension**	**Aquatic Vegetation Growth**	**Algae Degradation**	**Algae Growth**	**No Change**	**Total**
Reef sediments extension	67	0	3	0	55	125
Aquatic vegetation growth	0	4	0	0	4	8
Algae degradation	0	0	7	0	10	17
Algae growth	0	8	1	189	389	587
No change	4	4	7	51	5832	5898
Total	71	16	18	240	6290	6635
PA (%)	94.4	25	38.9	78.8	92.7	
UA (%)	53.6	50	41.2	32.2	98.9	
Object Area (m^2)	**Reef Sediments Extension**	**Aquatic Vegetation Growth**	**Algae Degradation**	**Algae Growth**	**No Change**	**Total**
Reef sediments extension	16,801.0	0.0	385.3	8.8	10,975.3	28,170.3
Aquatic vegetation growth	0.0	4283.2	0.0	446.8	1715.5	6445.5
Algae degradation	0.0	0.0	4202.0	125.3	2392.5	6719.8
Algae growth	9.8	1538.2	378.0	56,388.9	82,227.6	140,542.5
No change	3503.6	1654.2	3041.3	16,045.6	2,044,158.7	2,068,403.3
Total	20,314.3	7475.6	8006.5	73,015.3	2,141,469.5	2,250,281.3
PA (%)	82.7	57.3	52.5	77.2	95.5	
UA (%)	59.6	66.5	62.5	40.1	98.8	

Table 7. Confusion matrices of PBCD and OBCD results for Barque Canada Reef Site 2.

Barque Canada Reef Site 2	Reference				
Pixel Number	**Reef Sediments Extension**	**Aquatic Vegetation Growth**	**Algae Growth**	**No Change**	**Total**
Reef sediments extension	5356	36	0	13,995	19,387
Aquatic vegetation growth	8	6919	648	39,685	47,260
Algae growth	0	1519	3240	939	5698
No change	252	1803	137	246,847	249,039
Total	5616	10,277	4025	301,466	321,384
PA (%)	95.4	67.3	80.5	81.9	
UA (%)	27.6	14.6	56.9	99.1	
Object Number	**Reef Sediments Extension**	**Aquatic Vegetation Growth**	**Algae Growth**	**No Change**	**Total**
Reef sediments extension	102	0	0	206	308
Aquatic vegetation growth	0	167	17	187	371
Algae growth	0	10	42	19	71
No change	0	14	2	7253	7269
Total	102	191	61	7665	8019
PA (%)	100	87.4	68.9	94.6	
UA (%)	33.1	45	59.2	99.8	
Object Area (m^2)	**Reef Sediments Extension**	**Aquatic Vegetation Growth**	**Algae Growth**	**No Change**	**Total**
Reef sediments extension	27,893.8	0.0	0.0	39,508.3	67,402.0
Aquatic vegetation growth	0.0	94,803.5	2853.3	51,576.4	149,233.2
Algae growth	0.0	2788.3	18,071.5	3957.3	24,817.0
No change	0.0	5759.0	467.5	3,000,580.8	3,006,807.2
Total	27,893.8	103,350.7	21,392.3	3,095,622.7	3,248,259.5
PA (%)	100	91.7	84.5	96.9	
UA (%)	41.4	63.5	72.8	99.8	

3.2.2. Z-Test Results of the Accuracy Assessment

As shown in Table 8, the Z-test values of all the individual confusion matrices (especially the area-based OBCD confusion matrices) far exceeded 2.58 ($p \leq 0.01$) and 1.96 ($p \leq 0.05$), indicating that the RF algorithm combined PBCD and OBCD methods are both feasible and effective, and that the change detection results were significantly better than random results. Comparisons between the object-number-based OBCD assessment result and the PBCD assessment result revealed no significant differences for Zhongye Island ($|Z| = 0.60 < 1.69$), but the Z-test values for the other study sites were much larger than 2.58 ($p \leq 0.01$) and 1.96 ($p \leq 0.05$). Comparing the object-area-based assessment results and the pixel-number-based results, the Z-test values for all study sites were far greater than 2.58 ($p \leq 0.01$) and 1.96 ($p \leq 0.05$), i.e., the object-area-based accuracy was significantly higher than that of PBCD.

Table 8. Z-test results of individual confusion matrix and two confusion matrices.

	$\|Z\|$ [1]		Zhongye Island	Taiping Island	Barque Canada Reef	
					Site 1	Site 2
PBCD	Pixel-number-based	individual	178.36	102.84	63.41	135.87
OBCD	Object-number-based	individual	38.67	18.64	24.55	32.12
		OBCD vs. PBCD	7.40	0.60	17.60	14.38
	Object-area-based	individual	802.98	335.37	488.63	880.72
		OBCD vs. PBCD	60.47	19.36	175.99	165.59

[1] $|Z| \geq 2.58$ (1.69) denotes significant at the 99% (95%) confidence level.

4. Discussion

4.1. Pros and Cons of the Proposed OBCD Method

The proposed OBCD method segmented images from two different times together and then trained RF models using difference of object features to predict change category. The advantages of this method are evident. First, since change categories were defined in advance, changed areas and the corresponding change categories can be directly recognized using a one-step supervised classification. Secondly, the RF algorithm has high computational speed and helps optimizing the classification model by using only the input object features as predictive variables [65] compared to traditional rule-based method or pixel-based method. Changes can be detected in a more automatic way than with the membership rules method, which sets individual threshold values of classification rules iteratively based on expert knowledge and by visually comparing the image objects with field data [17,18]. Moreover, the algorithm running time of OBCD is obviously shorter than that of PBCD. In the PBCD method, the training sample size generally amounts to tens of thousands of pixels, while the training sample size for the OBCD method were only tens or hundreds of objects. Therefore, the average running time of the RF model for PBCD is about hundreds of seconds, while RF model building and change prediction could be accomplished within seconds for the OBCD method (not shown here). Thirdly, the method also achieved a high change detection accuracy (over 85%) for all the coral reef study sites, which confirms a good transferability of this workflow.

The proposed method also has some weakness. Small or indistinct changes cannot be easily detected due to the multi-temporal segmentation, where these changes may be merged into large objects in the segmentation process [72]. Despite the high overall accuracy, there was a great difference between per-class accuracy. Expect for the "no change" category, accuracies of other change categories were not as high as the accuracy recommended for creating an inventory of resources for management [73]. The imbalance of samples may have influence on the per-class accuracy. Classification trees suffer from unbalanced sample sizes because the largest number of samples tend to determine the class label [74]. On the other hand, challenges in respect of the quantity and quality of the training samples also affect the performance of the supervised classification [75]. In the reef island sites,

the "others" category always had the lowest accuracy, while the "no change" type, which accounted for the largest area of each study site, gained the highest accuracy. Changes of the "others" type relate to human development and reconstruction activities. Buildings and infrastructures on reef islands take various shapes and forms with distinctive spectral and textural properties, which greatly increased the uncertainty of the training samples in the supervised change detection. In addition, the number of training samples of "others" type obtained via proportional stratified sampling was quite small because of the limited extent of the changes. For example, in Taiping Island, the training samples of "others" type were 52 objects for object-based change detection and 357 pixels for pixel-based method as the area of "others" change type occupied only 4.98% of the entire study site. By contrast, there were 684 training objects and 13,218 training pixels of "no change" type.

4.2. The Superiority of the OBCD Method to the PBCD Method

A comparison of PBCD and OBCD showed that object-based paradigm is superior to the pixel-based paradigm for detecting changes from very-high-resolution satellite images of coral reefs. The OA of the OBCD method was about 20% greater than the PBCD method, similar to the findings derived by Benfield et al. [30] in their coral reef classification study. Cleve et al. [76] also found that the object-based classification approach provided a 17.97% higher OA than the pixel-based approach in wildland–urban interface classification. However, studies based on medium-resolution satellites such as Landsat and SPOT, concluded that the results achieved by pixel-based methods are acceptable, with no significant difference from the object-based methods [28,31]. As the spatial resolution of remote sensing imagery continues to improve, within-class spectral heterogeneities increase as well, which greatly affect the accuracy of conventional pixel-based methods. In this study, this problem was manifested in the form of severe salt-and-pepper effects and numerous misidentified pixels in the PBCD maps. The PBCD method recognizes changes based solely on pixel values, which are susceptible to interference from other factors. Factors including light conditions, tree shade, vegetation phenology, etc. might induce changes in the spectral features of pixels, thus leading to the detection of spurious changes. By comparison, the OBCD method analyzes the overall properties of all pixels within an object. Thus, changes of individual pixels have minimal impact on the general features of an object, making the OBCD method more robust and reliable.

4.3. Application of PBCD and OBCD Methods in Multiple Coral Reef Study Areas

The complicated formation process and the special location render coral reef islands spatiotemporally dynamic [77] and vulnerable to climate change and sea level rise [78]. Much attention has been paid to the dynamics of atoll islands. Historical aerial photographs or satellite images with different spatial resolution over a period of time were usually rectified to each other and digitalized to investigate the stability of vegetated cays or islands [79]. However, in most cases, atoll islands have a paucity of distinct and stable features for ground control points, rendering georeferencing of images problematic [80]. Besides, differing resolution or quality of time series images may affect the accuracy of the image registration and shoreline interpretation, and thus impact change detection accuracy. In our study, the proposed OBCD method was less prone to image misregistration than the PBCD method, as was observed from both the generated map and the accuracy. Using the PBCD method, pixels between neighboring segments tended to be misclassified, generating an obvious dividing line with a width of several pixels (Figure 7). Using the OBCD method, registration error did not cause fragmented objects. According to Chen, Zhao, and Powers [21], when the registration error is relatively small (e.g., lower than 3 pixels), the size of image objects slightly increased, because small objects were merged into the neighboring image-objects. Since misregistration had a low impact on object size and shape for most areas, the change detection accuracy would remain at a high level.

For the Barque Canada Reef study sites, it was found that PBCD methods were less suitable for coral reef community at a coarse scale, due to the serious salt and pepper effects in the change detection maps. In addition, it was found challenging to distinguish "aquatic vegetation growth" and "algae

growth". Seagrass and algae may have similar textural features and similar spectral characteristics using only the red, green, and blue bands. It has been suggested that hyperspectral data could provide for a more detailed and accurate classification or change detection of reef biotic systems, because it can provide rich information on the reflectance properties of algal and seagrass communities [81].

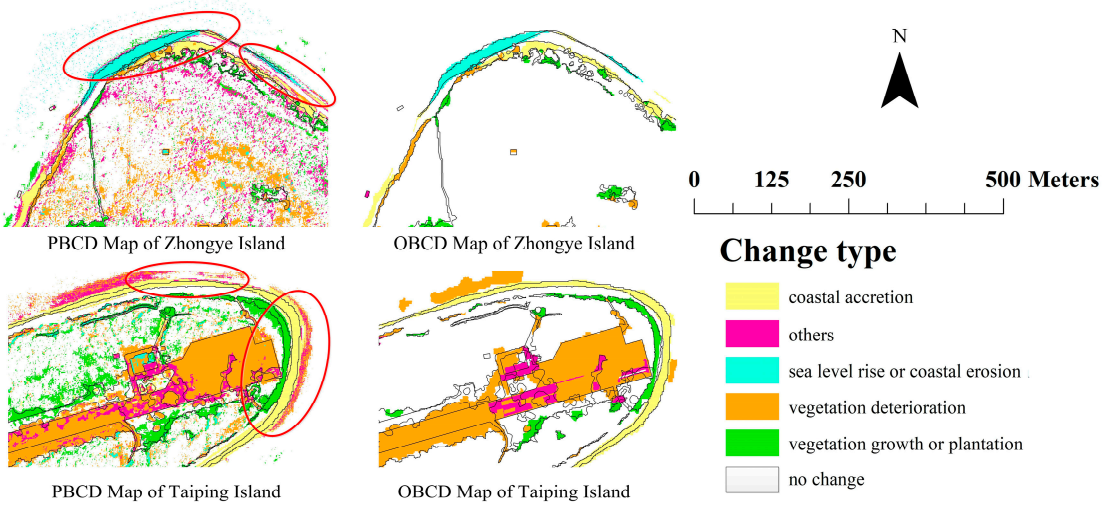

Figure 7. The impact of registration error on PBCD and OBCD change detection methods. (Pixels between neighboring segments were marked by red circle in PBCD change detection maps).

4.4. Object-Number-Based and Object-Area-Based Accuracy Assessment

In this work, we used two different accuracy assessment methods to evaluate the OBCD results. The object-area-based assessment of OBCD got a slightly higher OA than the object-number-based assessment and a greatly higher OA than the pixel-number-based assessment. Besides, the per-class accuracy of each change category was higher and more balanced in the object-area-based assessment. Although the OA of the object-number-based assessment was also greatly higher than the per-pixel results, the per-class accuracy did not show superiority. Two main reasons may account for all the findings above. First, in the object-based paradigm, image segmentation inevitably results in mixed objects; thus, once an object is misidentified, the object-number-based change detection accuracy will be lowered significantly, especially for change types with a small number of total samples. Second, the average size of correctly identified objects might be bigger than objects of incorrectly identified objects in almost all classes [82], so the final overall accuracy of object-area-based assessment was higher than the object-number-based accuracy. If the classified objects are imported to GIS for a further spatial analysis, both the thematic and geometric accuracy assessment are necessary and important. The object-area-based assessment is essentially a comprehensive evaluation of image segmentation and change detection, which is not only influenced by the classification algorithm, but also strongly relates to the segmentation means. Therefore, more combinations of classification algorithms and segmentation means need to be further explored.

5. Conclusions

As image registration is critical but challenging in coral reef change detection because of the deficiency of distinct and stable texture features as well as ground control points, in this work, we proposed an RF-combined object-based framework for change detection in coral reef environment and we applied this framework to multiple coral reef study sites in the South China Sea. The combination of multi-temporal object-based analysis and the RF algorithm not only recognized changed areas, but also offered information about the corresponding change types. The OBCD method achieved a high accuracy in coral reef environment with a good transferability over various study sites.

Through a comparison analysis, it was found that the OBCD method significantly outperformed the PBCD method. The OBCD method did not suffer from salt-and-pepper effects and it was less sensitive to image misregistration than the PBCD method. Therefore, the OBCD method is more suitable for coral reef environment monitoring. The object-area-based assessment of OBCD produced a higher OA than both the object-number-based assessment and the pixel-number-based assessment. Besides, per-class accuracy of the object-area-based assessment was higher and more balanced. For further GIS analysis or statistical analysis, the object-area-based accuracy assessment should be considered.

There were some shortcomings of this work. Given the high cost of field data collection, we had to visually interpret digitized high-resolution remote sensing images to obtain the reference layers. Thus, the change detection scale of this study was relatively coarse and the classification system of the change types was simple, especially for the Barque Canada Reef study sites. In future work, this framework could be tested on other coral reef images with rich validation information to realize change detection on finer scales with finer classification systems.

Author Contributions: All authors contributed to this paper. L.M. conceived and designed the experiments, and also contribute to the manuscript writing; Z.Z. performed the experiments, results interpretation, and manuscript writing; T.F., M.Y. and G.Z. assisted with the experimental result analysis; M.L. contributed images/materials/analysis tools.

Funding: This work was supported by the National Key R&D Program of China (No. 2017YFB0504200), the National Natural Science Foundation of China (No. 41701374), the Natural Science Foundation of Jiangsu Province of China (No. BK20170640), and the China Postdoctoral Science Foundation (No. 2017T10034, 2016M600392).

Acknowledgments: We are grateful to anonymous reviewers and members of the editorial team for advice.

Conflicts of Interest: The authors declare no conflict of interest.

Appendix A

Table A1. The area and proportion of reef island surface and coral reef habitats.

Zhongye Island				
Types	**Area in 2005 (m^2)**	**Proportion in 2005 (%)**	**Area in 2010 (m^2)**	**Proportion in 2010 (%)**
Buildings and infrastructures	154,819.86	24.85	145,485.35	23.35
Ocean	237,918.29	38.18	237,576.74	38.13
Bare land	35,529.86	5.70	35,064.84	5.63
Beach	20,092.13	3.22	26,716.40	4.29
Vegetation	174,709.09	28.04	178,225.91	28.60
Sum	623,069.23	100.00	623,069.23	100.00
Taiping Island				
Types	**Area in 2004 (m^2)**	**Proportion in 2004 (%)**	**Area in 2010 (m^2)**	**Proportion in 2010 (%)**
Buildings and infrastructures	67,932.38	9.17	127,455.08	17.20
Ocean	323,486.86	43.65	313,509.64	42.31
Bare land	34,235.36	4.62	42,485.03	5.73
Beach	37,762.43	5.10	50,523.22	6.82
Vegetation	277,608.10	37.46	207,052.17	27.94
Sum	741,025.13	100.00	741,025.13	100.00

Table A1. *Cont.*

Barque Canada Reef Site 1				
Types	**Area in 2013 (m^2)**	**Proportion in 2013 (%)**	**Area in 2015 (m^2)**	**Proportion in 2015 (%)**
Algae-dominated	117,799.30	5.23	316,069.08	14.04
Lagoon	235,411.50	10.46	7519.96	0.33
Ocean	462,830.44	20.56	220,900.08	9.81
Coral-dominated	270,640.08	12.02	241,113.99	10.71
Sand	400,262.34	17.78	485,582.71	21.57
Rubble-dominated	763,992.35	33.94	225,862.78	10.03
Aquatic vegetation	—	—	753,887.39	33.49
Sum	2,250,936.00	100.00	2,250,936.00	100.00
Barque Canada Reef Site 2				
Types	**Area in 2013 (m^2)**	**Proportion in 2013 (%)**	**Area in 2015 (m^2)**	**Proportion in 2015 (%)**
Algae-dominated	11679.00	0.36	33,324.13	1.03
Ocean	715,696.91	22.03	720,942.45	22.19
Coral-dominated	551,229.00	16.97	500,371.97	15.40
Rubble-dominated	868,028.67	26.72	892,846.00	27.48
Sand	1,102,457.99	33.93	1,000,743.93	30.80
Aquatic vegetation	—	—	100,863.09	3.10
Sum	3,249,091.57	100.00	3,249,091.57	100.00

Table A2. The area and proportion of all change categories in Zhongye Island and Taiping Island.

Change Categories	**Zhongye Island**		**Taiping Island**	
	Area (m^2)	**Proportion (%)**	**Area (m^2)**	**Proportion (%)**
Coastal accretion	13,485.46	2.16	16,761.46	2.26
No change	517,984.69	83.13	577,412.20	77.92
Others	1490.03	0.24	36,902.00	4.98
Sea level rise or coastal erosion	5327.20	0.85	2813.15	0.38
Vegetation deterioration	39,262.32	6.30	81,149.28	10.95
Vegetation growth or plantation	45,519.53	7.31	25,987.05	3.51
Sum	623,069.23	100.00	741,025.13	100.00

Table A3. The area and proportion of all change categories in Barque Canada Reef.

Change Categories	**Barque Canada Reef Site 1**		**Barque Canada Reef Site 2**	
	Area (m^2)	**Proportion (%)**	**Area (m^2)**	**Proportion (%)**
Algae growth	73,015.26	3.24%	21,655.81	0.67
Aquatic vegetation growth	7475.63	0.33%	100,852.41	3.10
Reef sediments extension	20,314.33	0.90%	30,428.52	0.94
Algae degradation	8006.50	0.36%	—	—
No change	2,141,469.54	95.16%	3,096,154.87	95.29
Sum	2,250,281.25	100.00%	3,249,091.60	100.00

Table A4. The object sample numbers of all change categories in Zhongye Island and Taiping Island.

Change Categories	**Zhongye Island**		**Taiping Island**	
	Training	**Validation**	**Training**	**Validation**
Coastal accretion	17	39	28	66
No change	1023	2386	684	1596
Others	2	5	52	121
Sea level rise or coastal erosion	11	26	5	12
Vegetation deterioration	21	48	100	234
Vegetation growth or plantation	28	65	33	76
Sum	1101	2569	902	2105

Table A5. The object sample numbers of all change categories in Barque Canada Reef.

Change Categories	Barque Canada Reef Site 1		Barque Canada Reef Site 2	
	Training	Validation	Training	Validation
Algae growth	103	240	40	93
Aquatic vegetation growth	7	16	128	299
Reef sediments extension	30	71	69	161
Algae degradation	8	18	—	—
No change	2695	6290	3199	7466
Sum	2843	6635	3436	8019

Table A6. The pixel sample numbers of all change categories in Zhongye Island and Taiping Island.

Change Categories	Zhongye Island		Taiping Island	
	Training	Validation	Training	Validation
Coastal accretion	453	1058	1241	2895
No change	9828	22,933	13,218	30,843
Others	72	169	357	834
Sea level rise or coastal erosion	191	446	1376	3211
Vegetation deterioration	765	1784	3111	7259
Vegetation growth or plantation	1373	3203	1650	3850
Sum	12,683	29,593	20,954	48,892

Table A7. The pixel sample numbers of all change categories in Barque Canada Reef.

Change Categories	Barque Canada Reef Site 1		Barque Canada Reef Site 2	
	Training	Validation	Training	Validation
Algae growth	6518	15,209	1725	4025
Aquatic vegetation growth	471	1098	4404	10,277
Reef sediments extension	1814	4233	2407	5616
Algae degradation	645	1506	—	—
No change	128,840	300,626	129,200	301,466
Sum	138,288	322,672	137,736	321,384

References

1. Moberg, F.; Folke, C. Ecological goods and services of coral reef ecosystems. *Ecol. Econ.* **1999**, *29*, 215–233. [CrossRef]
2. Reaka-Kudla, M.L. The global biodiversity of coral reefs: A comparison with rain forests. In *Biodiversity II: Understanding & Protecting Our Biological Resource*, 2nd ed.; Reaka-Kudla, M.L., Wilson, D.E., Wilson, E.O., Eds.; Joseph Henry/National Academy Press: Washington, DC, USA, 1997; pp. 83–108.
3. Folke, C. Confronting the coral reef crisis. *Nature* **2004**, *429*, 827.
4. Burke, L.M.; Reytar, K.; Spalding, M.; Perry, A.L. Reefs at risk revisited. *Ethics Medics* **2011**, *22*, 2008–2010.
5. McCarthy, M.J.; Colna, K.E.; El-Mezayen, M.M.; Laureano-Rosario, A.E.; Mendez-Lazaro, P.; Otis, D.B.; Toro-Farmer, G.; Vega-Rodriguez, M.; Muller-Karger, F.E. Satellite remote sensing for coastal management: A review of successful applications. *Environ. Manag.* **2017**, *60*, 323–339. [CrossRef] [PubMed]
6. Yamano, H.; Tamura, M. Detection limits of coral reef bleaching by satellite remote sensing: Simulation and data analysis. *Remote Sens. Environ.* **2004**, *90*, 86–103. [CrossRef]
7. Palandro, D.A.; Andréfouët, S.; Hu, C.; Hallock, P.; Müller-Karger, F.E.; Dustan, P.; Callahan, M.K.; Kranenburg, C.; Beaver, C.R. Quantification of two decades of shallow-water coral reef habitat decline in the florida keys national marine sanctuary using landsat data (1984–2002). *Remote Sens. Environ.* **2008**, *112*, 3388–3399. [CrossRef]
8. El-Askary, H.; Abd El-Mawla, S.H.; Li, J.; El-Hattab, M.M.; El-Raey, M. Change detection of coral reef habitat using landsat-5 TM, Landsat 7 ETM+ and Landsat 8 OLI data in the red sea (Hurghada, Egypt). *Int. J. Remote Sens.* **2014**, *35*, 2327–2346.

9. Mumby, P.J.; Green, E.P.; Edwards, A.J.; Clark, C.D. The cost-effectiveness of remote sensing for tropical coastal resources assessment and management. *J. Environ. Manag.* **1999**, *55*, 157–166. [CrossRef]
10. Scopélitis, J.; Andréfouët, S.; Phinn, S.; Done, T.; Chabanet, P. Coral colonisation of a shallow reef flat in response to rising sea level: Quantification from 35-years of remote sensing data at Heron Island, Australia. *Coral Reefs* **2011**, *30*, 951–965. [CrossRef]
11. Mumby, P.J.; Edwards, A.J. Mapping marine environments with ikonos imagery: Enhanced spatial resolution can deliver greater thematic accuracy. *Remote Sens. Environ.* **2002**, *82*, 248–257. [CrossRef]
12. Chen, G.; Hay, G.J.; Carvalho, L.M.T.; Wulder, M.A. Object-based change detection. *Int. J. Remote Sens.* **2012**, *33*, 4434–4457. [CrossRef]
13. Blaschke, T. Object based image analysis for remote sensing. *ISPRS J. Photogramm.* **2010**, *65*, 2–16. [CrossRef]
14. Zhang, C. Multiscale quantification of urban composition from EO-1/hyperion data using object-based spectral unmixing. *Int. J. Appl. Earth Obs. Geoinf.* **2016**, *47*, 153–162. [CrossRef]
15. Cheng, L.; Pian, Y.; Chen, Z.; Jiang, P.; Liu, Y.; Chen, G.; Du, P.; Li, M. Hierarchical filtering strategy for registration of remote sensing images of coral reefs. *IEEE J.-Stars* **2016**, *9*, 3304–3313. [CrossRef]
16. Leon, J.; Woodroffe, C.D. Improving the synoptic mapping of coral reef geomorphology using object-based image analysis. *Int. J. Geogr. Inf. Sci.* **2011**, *25*, 949–969. [CrossRef]
17. Phinn, S.R.; Roelfsema, C.M.; Mumby, P.J. Multi-scale, object-based image analysis for mapping geomorphic and ecological zones on coral reefs. *Int. J. Remote Sens.* **2012**, *33*, 3768–3797. [CrossRef]
18. Roelfsema, C.; Phinn, S.; Jupiter, S.; Comley, J.; Albert, S. Mapping coral reefs at reef to reef-system scales, 10s–1000s km^2, using object-based image analysis. *Int. J. Remote Sens.* **2013**, *34*, 6367–6388. [CrossRef]
19. Desclée, B.; Bogaert, P.; Defourny, P. Forest change detection by statistical object-based method. *Remote Sens. Environ.* **2006**, *102*, 1–11. [CrossRef]
20. Stow, D.A. Reducing the effects of misregistration on pixel-level change detection. *Int. J. Remote Sens.* **1999**, *20*, 2477–2483. [CrossRef]
21. Chen, G.; Zhao, K.; Powers, R. Assessment of the image misregistration effects on object-based change detection. *ISPRS J. Photogramm. Remote Sens.* **2014**, *87*, 19–27. [CrossRef]
22. Stow, D. Geographic object-based image change analysis. In *Handbook of Applied Spatial Analysis: Software Tools, Methods and Applications*; Fischer, M.M., Getis, A., Eds.; Springer: Berlin/Heidelberg, Germany, 2010; pp. 565–582.
23. Hussain, M.; Chen, D.; Cheng, A.; Wei, H.; Stanley, D. Change detection from remotely sensed images: From pixel-based to object-based approaches. *ISPRS J. Photogramm. Remote Sens.* **2013**, *80*, 91–106. [CrossRef]
24. Bontemps, S.; Bogaert, P.; Titeux, N.; Defourny, P. An object-based change detection method accounting for temporal dependences in time series with medium to coarse spatial resolution. *Remote Sens. Environ.* **2008**, *112*, 3181–3191. [CrossRef]
25. Niemeyer, I.; Marpu, P.R.; Nussbaum, S. *Change Detection Using Object Features*; Springer: Berlin/Heidelberg, Germany, 2008; pp. 185–201.
26. Lu, D.; Li, G.; Moran, E. Current situation and needs of change detection techniques. *Int. J. Image Data Fusion* **2014**, *5*, 13–38. [CrossRef]
27. Weih, R.C.; Riggan, N.D. Object-based classification vs. Pixel-based classification: Comparitive importance of multi-resolution imagery. In Proceedings of the GEOBIA 2010: Geographic Object-Based Image Analysis, Ghent, Belgium, 29 June–2 July 2010; p. 6.
28. Dingle Robertson, L.; King, D.J. Comparison of pixel- and object-based classification in land cover change mapping. *Int. J. Remote Sens.* **2011**, *32*, 1505–1529. [CrossRef]
29. Mafanya, M.; Tsele, P.; Botai, J.; Manyama, P.; Swart, B.; Monate, T. Evaluating pixel and object based image classification techniques for mapping plant invasions from uav derived aerial imagery: Harrisia pomanensis as a case study. *ISPRS J. Photogramm. Remote Sens.* **2017**, *129*, 1–11. [CrossRef]
30. Benfield, S.L.; Guzman, H.M.; Mair, J.M.; Young, J.A.T. Mapping the distribution of coral reefs and associated sublittoral habitats in pacific panama: A comparison of optical satellite sensors and classification methodologies. *Int. J. Remote Sens.* **2007**, *28*, 5047–5070. [CrossRef]
31. Duro, D.C.; Franklin, S.E.; Dubé, M.G. A comparison of pixel-based and object-based image analysis with selected machine learning algorithms for the classification of agricultural landscapes using SPOT-5 HRG imagery. *Remote Sens. Environ.* **2012**, *118*, 259–272. [CrossRef]

32. Huang, D.; Licuanan, W.Y.; Hoeksema, B.W.; Chen, C.A.; Ang, P.O.; Huang, H.; Lane, D.J.W.; Vo, S.T.; Waheed, Z.; Affendi, Y.A.; et al. Extraordinary diversity of reef corals in the south China sea. *Mar. Biodivers.* **2015**, *45*, 157–168. [CrossRef]
33. Morton, B.; Blackmore, G. South China sea. *Mar. Pollut. Bull.* **2001**, *42*, 1236–1263. [CrossRef]
34. Cooley, T.; Anderson, G.P.; Felde, G.W.; Hoke, M.L.; Ratkowski, A.J.; Chetwynd, J.H.; Gardner, J.A.; Adler-Golden, S.M.; Matthew, M.W.; Berk, A.; et al. FLAASH, a MODTRAN4-based atmospheric correction algorithm, its application and validation. In Proceedings of the IEEE International Geoscience and Remote Sensing Symposium, Toronto, ON, Canada, 24–28 June 2002; pp. 1414–1418.
35. ITT Visual Information Solutions. FLAASH Module. In *Atmospheric Correction Module: QUAC and FLAASH User's Guide*; Version 4.7; ITT Visual Information Solutions: Boulder, CO, USA, 2009; p. 44.
36. Aiazzi, B.; Baronti, S.; Selva, M.; Alparone, L. Enhanced gram-schmidt spectral sharpening based on multivariate regression of MS and Pan data. In Proceedings of the 2006 IEEE International Symposium on Geoscience and Remote Sensing, Denver, CO, USA, 31 July–4 August 2006; pp. 3806–3809.
37. Lyzenga, D.R. Remote sensing of bottom reflectance and water attenuation parameters in shallow water using aircraft and landsat data. *Int. J. Remote Sens.* **1981**, *2*, 71–82. [CrossRef]
38. Andréfouët, S. Coral reef habitat mapping using remote sensing: A user vs producer perspective. Implications for research, management and capacity building. *J. Spat. Sci.* **2008**, *53*, 113–129. [CrossRef]
39. Mumby, P.J.; Green, E.P.; Edwards, A.J.; Clark, C.D. Coral reef habitat mapping: How much detail can remote sensing provide? *Mar. Biol.* **1997**, *130*, 193–202. [CrossRef]
40. Neubert, M.; Herold, H.; Meinel, G. Evaluation of remote sensing image segmentation quality–further results and concepts. In Proceedings of the 1 St International Conference on Object-based Image Analysis, Gvttingen, Germany, 7–8 October 2005.
41. Baatz, M.; Schäpe, A. An optimization approach for high quality multi-scale image segmentation. In Proceedings of the Beiträge zum AGIT-Symposium, Salzburg, Germany, 3–5 July 2000; pp. 12–23.
42. Woodcock, C.E.; Strahler, A.H. The factor of scale in remote sensing. *Remote Sens. Environ.* **1987**, *21*, 311–332. [CrossRef]
43. Drăguţ, L.; Csillik, O.; Eisank, C.; Tiede, D. Automated parameterisation for multi-scale image segmentation on multiple layers. *ISPRS J. Photogramm. Remote Sens.* **2014**, *88*, 119–127. [CrossRef] [PubMed]
44. Drăguţ, L.; Tiede, D.; Levick, S.R. Esp: A tool to estimate scale parameter for multiresolution image segmentation of remotely sensed data. *Int. J. Geogr. Inf. Sci.* **2010**, *24*, 859–871. [CrossRef]
45. Bontemps, S.; Langner, A.; Defourny, P. Monitoring forest changes in borneo on a yearly basis by an object-based change detection algorithm using SPOT-vegetation time series. *Int. J. Remote Sens.* **2012**, *33*, 4673–4699. [CrossRef]
46. Lillesand, T.M.; Kiefer, R.W. *Remote Sensing and Image Interpretation*; John Wiley and Sons: New York, NY, USA, 2008.
47. Boulila, W.; Farah, I.R.; Ettabaa, K.S.; Solaiman, B.; Ghézala, H.B. A data mining based approach to predict spatiotemporal changes in satellite images. *Int. J. Appl. Earth Obs. Geoinf.* **2011**, *13*, 386–395. [CrossRef]
48. Volpi, M.; Tuia, D.; Bovolo, F.; Kanevski, M.; Bruzzone, L. Supervised change detection in VHR images using contextual information and support vector machines. *Int. J. Appl. Earth Obs.* **2013**, *20*, 77–85. [CrossRef]
49. Tucker, C.J. Red and photographic infrared linear combinations for monitoring vegetation. *Remote Sens. Environ.* **1979**, *8*, 127–150. [CrossRef]
50. McFeeters, S.K. The use of the normalized difference water index (NDWI) in the delineation of open water features. *Int. J. Remote Sens.* **1996**, *17*, 1425–1432. [CrossRef]
51. Haralick, R.M.; Shanmugam, K.; Dinstein, I.H. Textural features for image classification. *IEEE Trans. Syst. Man Cybern.* **1973**, *smc-3*, 610–621. [CrossRef]
52. Breiman, L. Random forests. *Mach. Learn.* **2001**, *45*, 5–32. [CrossRef]
53. Chan, J.C.-W.; Paelinckx, D. Evaluation of random forest and adaboost tree-based ensemble classification and spectral band selection for ecotope mapping using airborne hyperspectral imagery. *Remote Sens. Environ.* **2008**, *112*, 2999–3011. [CrossRef]
54. Immitzer, M.; Atzberger, C.; Koukal, T. Tree species classification with random forest using very high spatial resolution 8-band WorldView-2 satellite data. *Remote. Sens.* **2012**, *4*, 2661. [CrossRef]
55. Gislason, P.O.; Benediktsson, J.A.; Sveinsson, J.R. Random forests for land cover classification. *Pattern Recogn. Lett.* **2006**, *27*, 294–300. [CrossRef]

56. Khatami, R.; Mountrakis, G.; Stehman, S.V. A meta-analysis of remote sensing research on supervised pixel-based land-cover image classification processes: General guidelines for practitioners and future research. *Remote Sens. Environ.* **2016**, *177*, 89–100. [CrossRef]
57. Ghosh, A.; Joshi, P.K. A comparison of selected classification algorithms for mapping bamboo patches in lower gangetic plains using very high resolution WorldView 2 imagery. *Int. J. Appl. Earth Obs. Geoinf.* **2014**, *26*, 298–311. [CrossRef]
58. Dalponte, M.; Ørka, H.O.; Gobakken, T.; Gianelle, D.; Næsset, E. Tree species classification in boreal forests with hyperspectral data. *IEEE Trans. Geosci. Remote Sens.* **2013**, *51*, 2632–2645. [CrossRef]
59. Sesnie, S.E.; Finegan, B.; Gessler, P.E.; Thessler, S.; Ramos Bendana, Z.; Smith, A.M.S. The multispectral separability of costa rican rainforest types with support vector machines and random forest decision trees. *Int. J. Remote Sens.* **2010**, *31*, 2885–2909. [CrossRef]
60. Pal, M. Random forest classifier for remote sensing classification. *Int. J. Remote Sens.* **2005**, *26*, 217–222. [CrossRef]
61. Mandianpari, M.; Salehi, B.; Mohammadimanesh, F.; Motagh, M. Random forest wetland classification using ALOS-2 L-band, RADARSAT-2 C-band, and TerraSAR-X imagery. *ISPRS J. Photogramm. Remote Sens.* **2017**, *130*, 13–31. [CrossRef]
62. Li, M.; Ma, L.; Blaschke, T.; Cheng, L.; Tiede, D. A systematic comparison of different object-based classification techniques using high spatial resolution imagery in agricultural environments. *Int. J. Appl. Earth Obs. Geoinf.* **2016**, *49*, 87–98. [CrossRef]
63. Ma, L.; Fu, T.; Blaschke, T.; Li, M.; Tiede, D.; Zhou, Z.; Ma, X.; Chen, D. Evaluation of feature selection methods for object-based land cover mapping of unmanned aerial vehicle imagery using random forest and support vector machine classifiers. *ISPRS Int. J. Geo-Inf.* **2017**, *6*, 51. [CrossRef]
64. Liaw, A.; Wiener, M. Classification and regression by randomforest. *R News* **2002**, *2*, 18–20.
65. Belgiu, M.; Drăguţ, L. Random forest in remote sensing: A review of applications and future directions. *ISPRS J. Photogramm. Remote Sens.* **2016**, *114*, 24–31. [CrossRef]
66. Rodriguez-Galiano, V.F.; Ghimire, B.; Rogan, J.; Chica-Olmo, M.; Rigol-Sanchez, J.P. An assessment of the effectiveness of a random forest classifier for land-cover classification. *ISPRS J. Photogramm. Remote Sens.* **2012**, *67*, 93–104. [CrossRef]
67. Laliberte, A.S.; Rango, A. Texture and scale in object-based analysis of subdecimeter resolution unmanned aerial vehicle (UAV) imagery. *IEEE Trans. Geosci. Remote Sens.* **2009**, *47*, 761–770. [CrossRef]
68. Schöpfer, E.; Lang, S.; Albrecht, F. *Object-Fate Analysis—Spatial Relationships for the Assessment of Object Transition and Correspondence*; Springer: Berlin/Heidelberg, Germany, 2008; pp. 785–801.
69. Freire, S.; Santos, T.; Navarro, A.; Soares, F.; Silva, J.D.; Afonso, N.; Fonseca, A.; Tenedório, J. Introducing mapping standards in the quality assessment of buildings extracted from very high resolution satellite imagery. *ISPRS J. Photogramm. Remote Sens.* **2014**, *90*, 1–9. [CrossRef]
70. Whiteside, T.G.; Maier, S.W.; Boggs, G.S. Area-based and location-based validation of classified image objects. *Int. J. Appl. Earth Obs.* **2014**, *28*, 117–130. [CrossRef]
71. Congalton, R.G.; Green, K. *Assessing the Accuracy of Remotely Sensed Data—Principles and Practices*, 2nd ed.; CRC Press: Boca Raton, FL, USA, 2009; p. 183.
72. Tewkesbury, A.P.; Comber, A.J.; Tate, N.J.; Lamb, A.; Fisher, P.F. A critical synthesis of remotely sensed optical image change detection techniques. *Remote Sens. Environ.* **2015**, *160*, 1–14. [CrossRef]
73. Green, E.P.; Edwards, A.J. *Remote Sensing Handbook for Tropical Coastal Management*; UNESCO: Paris, France, 2000; pp. 141–154.
74. Hansen, M.C.; Defries, R.S.; Townshend, J.R.G.; Sohlberg, R. Global land cover classification at 1 km spatial resolution using a classification tree approach. *Int. J. Remote Sens.* **2000**, *21*, 1331–1364. [CrossRef]
75. Chegoonian, A.M.; Mokhtarzade, M.; Valadan Zoej, M.J. A comprehensive evaluation of classification algorithms for coral reef habitat mapping: Challenges related to quantity, quality, and impurity of training samples. *Int. J. Remote Sens.* **2017**, *38*, 4224–4243. [CrossRef]
76. Cleve, C.; Kelly, M.; Kearns, F.R.; Moritz, M. Classification of the wildland-urban interface: A comparison of pixel- and object-based classifications using high-resolution aerial photography. *Comput. Environ. Urban Syst.* **2008**, *32*, 317–326. [CrossRef]
77. Hamylton, S.M.; Puotinen, M. A meta-analysis of reef island response to environmental change on the great barrier reef. *Earth Surf. Process. Landf.* **2015**, *40*, 1006–1016. [CrossRef]

78. Webb, A.P.; Kench, P.S. The dynamic response of reef islands to sea-level rise: Evidence from multi-decadal analysis of island change in the central Pacific. *Glob. Planet. Chang.* **2010**, *72*, 234–246. [CrossRef]
79. Kayanne, H.; Aoki, K.; Suzuki, T.; Hongo, C.; Yamano, H.; Ide, Y.; Iwatsuka, Y.; Takahashi, K.; Katayama, H.; Sekimoto, T.; et al. Eco-geomorphic processes that maintain a small coral reef island: Ballast Island in the Ryukyu Islands, Japan. *Geomorphology* **2016**, *271*, 84–93. [CrossRef]
80. Ford, M. Shoreline changes interpreted from multi-temporal aerial photographs and high resolution satellite images: Wotje atoll, marshall islands. *Remote Sens. Environ.* **2013**, *135*, 130–140. [CrossRef]
81. Karpouzli, E.; Malthus, T.J.; Place, C.J. Hyperspectral discrimination of coral reef benthic communities in the western caribbean. *Coral Reefs* **2004**, *23*, 141–151. [CrossRef]
82. Myint, S.W.; Gober, P.; Brazel, A.; Grossman-Clarke, S.; Weng, Q. Per-pixel vs. Object-based classification of urban land cover extraction using high spatial resolution imagery. *Remote Sens. Environ.* **2011**, *115*, 1145–1161. [CrossRef]

© 2018 by the authors. Licensee MDPI, Basel, Switzerland. This article is an open access article distributed under the terms and conditions of the Creative Commons Attribution (CC BY) license (http://creativecommons.org/licenses/by/4.0/).